Monthly Notices
of the
ROYAL ASTRONOMICAL SOCIETY

MNRAS **483,** 1470–1480 (2019)
Advance Access publication 2018 November 27

doi:10.1093/mnras/sty3209

New candidates to polar-ring galaxies from the Sloan Digital Sky Survey

Vladimir P. Reshetnikov [1]★ and Aleksandr V. Mosenkov [2]★

[1] *St. Petersburg State University, 7/9 Universitetskaya nab., St. Petersburg 199034, Russia*
[2] *Central Astronomical Observatory, Russian Academy of Sciences, 65/1 Pulkovskoye chaussee, St. Petersburg 196140, Russia*

Accepted 2018 November 23. Received 2018 November 21; in original form 2018 March 16

ABSTRACT

Polar-ring galaxies (PRGs) are fascinating systems in which the central object (typically, an early-type galaxy) is encircled by a large-scale ring of stars, gas, and dust with almost perpendicular spin. PRGs are rare objects and their formation mechanism is not entirely clear. In this paper, we present a new sample of 31 candidates to PRGs identified in the Sloan Digital Sky Survey (SDSS). Using their stacked *gri*-images, we determined geometrical parameters of these galaxies; the position angle and the size of the host galaxy and the ring. We compare our sample objects to the previously known PRGs and discuss their general characteristics; the frequency of faint outer structures, the luminosity–size relation, and the distribution by the apparent angle between the ring and the host galaxy. Our main results are: (i) Central galaxies of PRGs follow the luminosity–size relation for ordinary galaxies. The ring components are located along the similar relation but with a larger scatter. This increasing scatter may be the result of a secondary origin of polar structures. (ii) At least half of PRGs show a ring component within 20° from the perpendicular orientation.

Key words: galaxies: interactions – galaxies: peculiar – galaxies: statistics.

1 INTRODUCTION

Polar-ring galaxies (PRGs) provide remarkable examples of the non-monotonicity of the galaxy formation process. Typically, they consist of two large-scale luminous subsystems: a central galaxy and a ring or a disc which are oriented nearly orthogonally to the major axis of the central object (see examples in the Whitmore et al. 1990 (=PRC) and Moiseev et al. 2011 (=SPRC) catalogues). In this article, we further use the term 'PRG' to designate a class of objects with near-polar optical structures – without dividing into polar-disc or polar-ring galaxies (see for instance, Iodice 2014).

In most cases, two subsystems in PRGs differ noticeably by their characteristics. The central (host) galaxies are typically early-type (E/S0) galaxies, poor in gas (Whitmore, McElroy & Schweizer 1987; Finkelman, Funes & Brosch 2012; Reshetnikov & Combes 2015). In contrast, the polar structures are generally younger, blue (e.g. Reshetnikov, Hagen-Thorn & Yakovleva 1994; Iodice et al. 2002), with large amount (several times $10^9\,M_\odot$) of HI (e.g. van Gorkom, Schechter & Kristian 1987; van Driel et al. 2000).

Various scenarios have been proposed to explain the formation of the two kinematically and morphologically decoupled structures in PRGs: the capture of matter from an approached galaxy (Reshetnikov & Sotnikova 1997; Bournaud & Combes 2003), the merging of galaxies (Bekki 1997, 1998; Bournaud & Combes 2003), the misaligned accretion of matter from cosmic filaments (e.g. Maccio, Moore & Stadel 2006; Brook et al. 2008), and some others. Observations show that several formation mechanisms can apparently be realized.

Galaxies with polar structures are an important class of objects that allows us to study a wide range of problems, linked with the formation and evolution of galaxies under external accretion, and to study the properties of their dark haloes. Unfortunately, PRGs are very rare objects, with a fraction of $\sim 10^{-3}$ of all galaxies in the local Universe (Whitmore et al. 1990; Reshetnikov, Faúndez-Abans & de Oliveira-Abans 2011). Consequently, most recent studies of PRGs are concentrated mainly on a few relatively nearby and bright galaxies: NGC 4650A (e.g. Coccato, Iodice & Arnaboldi 2014, Iodice et al. 2015), A0136-0801 (Spavone, Iodice & Arnaboldi 2015), NGC 660 (Smirnova, Wiebe & Moiseev 2017), and some others.

There were several attempts to collect large samples of such galaxies. Whitmore et al. (1990) have presented a photographic atlas of PRGs and related objects containing 157 galaxies but, according to further studies, only a small part of the atlas galaxies appeared to be true PRGs.

The next important step was the catalogue SPRC by Moiseev et al. (2011) based on the results from the Galaxy Zoo project[1] (Lintott et al. 2008). The SPRC catalogue contains 275 objects split into four groups. The first two groups comprise 'best candidates' (70 objects) and 'good candidates' (115 objects) for PRGs. The

★ E-mail: v.reshetnikov@spbu.ru (VPR); mosenkovav@gmail.com (AVM)

[1] http://www.galaxyzoo.org/

remaining objects are related galaxies (mergers, strong warps) and possible face-on polar rings. A further study showed that an appreciable fraction of the SPRC objects are indeed PRGs (fig. 1 in Moiseev et al. 2015 gives several examples).

In this work we present a new sample of 'best' and 'good' (in the sense of SPRC) candidates to PRGs. Our sample includes 31 galaxies compiled from Galaxy Zoo discussion boards.

Throughout this article, we adopt a standard flat ΛCDM cosmology with $\Omega_m = 0.3$, $\Omega_\Lambda = 0.7$, $H_0 = 70\,\mathrm{km\,s^{-1}\,Mpc^{-1}}$. All magnitudes in the paper are given in the AB-system.

2 THE SAMPLE AND DATA REDUCTION

2.1 The sample

To select new candidates to PRGs, we analysed discussion boards[2] of the Galaxy Zoo project. By eye looking at the morphology of these galaxies (using coloured SDSS snapshots), we finally selected a sample of 31 objects with a morphology resembling 'classical' PRGs, like A0136-0801, NGC 4650A, NGC 2685 (see Whitmore et al. 1990 catalogue). The selected objects show two inclined large-scale structures, the centres of which nearly coincide. The full list of galaxies, along with some of their general properties, which are derived in Section 2.3, is presented in Table 1. The reduced images of all candidates to PRGs are shown in the Appendix A, Fig. A1 (see the description of these images below).

We should notice that our selection is strongly biased due to the fact that only PRGs with highly inclined and extended polar structures (PS) can be easily found. As mentioned by Whitmore et al. (1990), PS that has a smaller diameter than the host galaxy (HG), i.e. a narrow polar ring, and that has a small inclination angle with respect to the HG are difficult to detect. This selected sample of galaxies cannot be completed by any means, and can only be considered as an extension of the already existing sample of candidates to this rare class of PRGs (see e.g. Moiseev et al. 2011).

Most objects in our sample look typical for PRGs – they possess an extended edge-on component which is almost orthogonal to the central galaxy. In two cases, the galaxies #15 (SDSS 112850.42−061614.1) and #16 (SDSS 124513.41−154102.0), the suspected PSs are moderately inclined to the line of sight. The galaxy #15 (SDSS 112850.42−061614.1) looks very similar to the kinematically confirmed polar-ring galaxy SPRC-7 (Brosch et al. 2010).

2.2 The data reduction

To highlight faint polar structures, which may be present in galaxies, we used the following technique adopted from Miskolczi, Bomans & Dettmar (2011). The system response curves of the SDSS imaging camera (Gunn et al. 1998) show that the highest values are reached in the filters *g*, *r*, and *i*, therefore we analysed the galaxy images in these three filters only. The corrected frames were directly downloaded from the SDSS archive, Data Release 12 (Alam et al. 2015). Most of the galaxies lie within one frame, but for those galaxies, which lie at the border of the frame, additional overlapping frames were downloaded and combined together using the SWARP routine (Bertin et al. 2002).

[2] https://talk.galaxyzoo.org/#/boards

Then we determined the radius $R_{2\sigma}$ of the circle which encompasses the 2σ-level isophote of the stacked *gri*-image (see below) of the galaxy, which was initially created from the directly downloaded images in the *g*, *r,* and *i* bands (no sky-background correction). After that, we created an initial mask using SEXTRACTOR (Bertin, Arnouts 1996) and applied sigma-clipping to estimate the median and standard deviation of the background in each band. Although SDSS frames have been already sky subtracted, we decided to re-estimate the background near each galaxy. For this purpose, to each galaxy frame we applied the IRAF*ellipse* routine to create the growth curve. Then we defined an annulus in which the background was carefully estimated (again, using sigma-clipping) as having the inner radius 1.50 $R_{2\sigma}$ and the outer radius 1.80 $R_{2\sigma}$. The area of the annulus in this case is equal to the area inside the circle which is circumscribed about the galaxy. We double checked that within this annulus the growth curve is flat. We did not apply the polynomial fitting of the sky background because the SDSS frames have been already sky subtracted and we found no gradient of the sky background. The calculated background (which appeared to be within 1 per cent of the background level which was determined in the SDSS) was then subtracted from each frame.

Asymptotic magnitudes in each band were estimated by extrapolating the dependence of the gradient d*m*/d*r* on magnitude to d*m*/d*r* = 0 (by definition, this gives the asymptotic magnitude of the galaxy, see e.g. Muñoz-Mateos et al. 2015). The estimated uncertainties in the magnitudes are a combination of the associated sky error value, the Poisson error on the incident flux, and the SDSS calibration error of 0.8 per cent (Alam et al. 2015). In addition, we also found the effective radius of each galaxy, using the created growth curves.

The obtained images in each filter were stacked together using the IRAF task *imcombine*. This was done in order to improve the signal-to-noise ratio of each individual image. After that, for all three filters we created individual mask images which contain contaminating stars and galaxies. This step was done using the segmentation maps, produced by SEXTRACTOR, which were then carefully revisited by eye to ensure that all foreground stars and galaxies had been removed from the galaxy images. However, we decided not to mask out close, overlapping galaxies (as in the case of SDSS J135711.99−070430.3) since the light from them non-negligibly affects the surface brightness distribution of the polar-ring galaxy. After that, to mask all contaminating pixels in the stacked galaxy image, the masks in all three filters were combined.

In the next step, to make faint features visible, we used a circularly symmetric Gaussian filter with σ = 2–4 pix; these values were found optimal for each galaxy to achieve a good enhancement of a faint ring structure. Since in the vicinity of the sample galaxies no bright stars are found on the final images (except for SDSS J105157.88+085122.0) and the galaxies are rather small, we did not found large gradients of the background. The radius $R_{2\sigma}$ was re-determined for the final *gri*-images.

In Fig. 1 we show a typical PRG in our sample, SDSS J091558.60+093455.3, whereas *gri*-images for all sample galaxies are given in the Appendix in Fig. A1. As can be seen, in some galaxies a PS is well prominent, whereas in others it is quite faint and barely visible.

2.3 The analysis of the images

To estimate the apparent position angle of the HG and PS, we applied the following approach. Since in most galaxies in our sample the PS looks as a rather faint almost orthogonally oriented structure, the

Table 1. General characteristics of the sample galaxies. The columns 4–11 are described in Section 2.2–2.3.

#	SDSS name	z	r_{as} (mag)	M_r^0	$(g-r)_0$	$R_{2\sigma}$ (kpc)	R_{eff} (kpc)	ΔP.A. (grad)	D_r (kpc)	D_r/D_h
(1)	(2)	(3)	(4)	(5)	(6)	(7)	(8)	(9)	(10)	(11)
1	001524.31+184624.8	0.0186	14.35 ± 0.02	−20.25	0.72	9.2	3.5	86	18.4	1.20
2	004914.26+120858.1	0.0383	14.57 ± 0.05	−21.71	0.77	12.8	2.6	81	24.8	1.00
3	010816.84−082317.6	0.0467	15.08 ± 0.03	−21.60	0.82	14.8	9.2	78	29.6	1.15
4	013905.96+192559.9	0.0880	16.38 ± 0.05	−21.78	0.72	13.2	4.8	87	26.4	1.16
5	015828.87+013549.9	0.0600	16.60 ± 0.06	−20.59	0.69	8.4	2.7	68	14.4	0.86
6	020316.58+293830.4	(0.038)	14.83 ± 0.04	–	0.72	–	–	79	–	0.45
7	041557.96−051655.8	0.0317	15.08 ± 0.03	−20.83	0.86	9.8	4.6	86	19.5	1.43
8	074308.88+240206.5	0.0880	16.88 ± 0.03	−21.27	0.66	26.7	8.1	88	53.4	4.06
9	075131.01+500216.7	0.0600	16.37 ± 0.08	−20.92	0.77	11.5	4.0	80	22.2	1.05
10	081740.08+042952.3	0.1100	17.01 ± 0.03	−21.66	0.82	14.3	6.4	81	28.5	1.26
11	091522.74+271711.9	0.0460	14.28 ± 0.02	−22.28	0.63	26.7	11.1	69	53.4	1.11
12	091558.60+093455.3	0.0450	15.92 ± 0.05	−20.67	0.79	12.8	2.1	78	25.6	1.82
13	105157.88+085122.0	0.0520	14.67 ± 0.02	−22.20	0.71	19.6	11.6	84	27.9	0.71
14	112301.31+470308.7	0.0250	14.32 ± 0.03	−20.86	0.75	9.0	3.5	85	18.0	1.07
15	112850.42−061614.1	0.0202	15.85 ± 0.03	−18.89	0.43	10.4	2.7	24	20.7	2.88
16	124513.41−154102.0	0.0440	14.76 ± 0.03	−21.76	0.63	18.8	6.4	70	37.6	1.52
17	133040.07+113541.7	0.0240	15.05 ± 0.02	−20.07	0.67	10.1	5.6	83	15.7	0.77
18	135711.99−070430.3	0.0275	14.17 ± 0.01	−21.28	1.03	8.4	11.4	52	7.6	0.45
19	140435.21+555536.8	(0.128)	18.22 ± 0.09	–	0.81	–	–	78	–	1.91
20	161103.94+140043.6	0.0310	15.86 ± 0.05	−19.86	0.62	6.5	2.5	64	12.9	1.28
21	162434.00+364015.5	0.0500	16.17 ± 0.08	−20.59	0.80	7.4	1.8	73	11.1	0.75
22	165057.26+044931.4	(0.071)	16.54 ± 0.01	–	0.52	–	–	61	–	0.90
23	175659.49+040143.3	(0.117)	17.47 ± 0.06	–	0.60	–	–	67	–	1.02
24	204425.23+022322.2	0.0595	16.28 ± 0.04	−21.06	0.56	13.1	5.2	63	17.6	0.67
25	205213.48+034924.3	(0.034)	16.22 ± 0.06	–	0.38	–	–	76	–	0.97
26	211245.01+092938.0	0.0960	17.05 ± 0.06	−21.46	0.67	13.5	3.7	72	27.2	1.30
27	220419.41+125806.2	0.0270	14.25 ± 0.03	−21.20	0.79	11.6	3.6	74	12.9	0.56
28	221126.92+175348.4	0.0200	16.60 ± 0.04	−18.16	0.77	4.3	1.5	53	8.6	1.78
29	224835.75+072424.8	(0.082)	16.74 ± 0.06	–	0.72	–	–	90	–	0.99
30	234407.32+253657.7	0.0960	16.00 ± 0.03	−22.37	0.80	18.6	8.8	88	37.2	1.50
31	234756.34+080151.4	(0.042)	15.00 ± 0.02	–	0.37	–	–	73	–	0.62

Columns: (1) designation number in the sample,
(2) SDSS name,
(3) spectroscopic redshift (SDSS or NED), brackets mark photometric redshifts (SDSS),
(4) asymptotic magnitude in the r band,
(5) absolute magnitude in the r band corrected for the Milky Way extinction (Schlafly & Finkbeiner 2011) and k-correction (Chilingarian, Melchior & Zolotukhin 2010),
(6) $g-r$ colour calculated from the corresponding asymptotic magnitudes and corrected for the Milky Way extinction (Schlafly & Finkbeiner 2011) and k-correction (Chilingarian et al. 2010),
(7) radius of the 2σ-isophote estimated for the stacked gri-image,
(8) effective radius in the r band,
(9) apparent angle between the ring and the central galaxy,
(10) diameter of the suspected ring,
(11) the ring diameter normalized by the diameter of the host galaxy.

proper way to determine the orientation of the host galaxy and the polar structure is by fitting the whole galaxy with a two-component model 'host + polar structure'. For this purpose, we used a new version of the DECA package (Mosenkov 2014) which was specially designed to perform automatic and semi-automatic decomposition of galaxy images on to several structural components. Most galaxies in our sample consist of a HG and a PS which can be both generally described by a Sérsic function (Sérsic 1968). This approximation is justified by the following reasons. First, the sample galaxies are rather small, and, thus, are poorly resolved to be properly fitted with a more complex model. Second, the polar structure in most galaxies from our sample is oriented in a way that no contrast ring is seen. But even in the case of SDSS J112850.42−061614.1 (where the PS is moderately inclined towards the observer and seen well), a model with a very small Sérsic index ($n < 0.1$) strives to fit the ring structure by making the central part of the model flat. This method has been tested successfully on a sample of galaxies with apparent ring structures in the far-infrared (Mosenkov et al. 2018). Also, since our aim is to merely estimate the position angles of almost orthogonal components, this rough fitting scheme allows us to do this very easily. Another way to find the position angles of the HG and PS would be using the distribution of the position angle by radius, which has been derived using the IRAF task *ellipse*. However, we found that since most PS in our sample are barely visible, this approach does not allow us to robustly determine the difference in the position angles at different radii, and, thus, clearly discern the HG and PS in the distributions of the position angle by radius.

In some galaxies additional components (apart from the HG and PS) were fitted with another Sérsic function to create a realistic

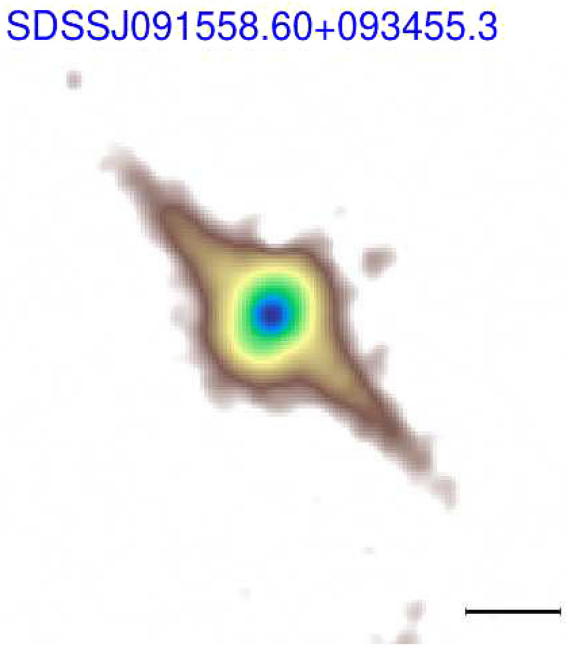

Figure 1. Reduced (stacked) *gri*-image of SDSS J091558.60+093455.3. The contaminating sources have been masked. The scale bar corresponds to 10 arcsec.

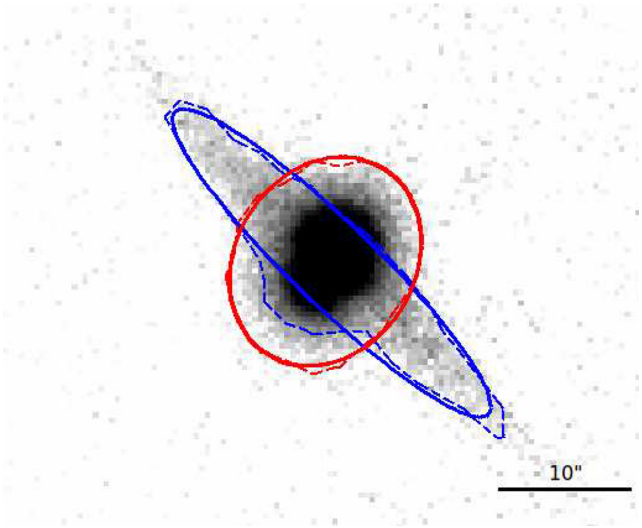

Figure 3. The results of the ellipse fitting for a stacked *gri*-image of the galaxy SDSS J091558.60+093455.3. The dashed contours are the outermost isophotes (at 2σ), which were created for the residual images 'galaxy – host' and 'galaxy – ring'. The red solid contour shows the fit ellipse for the HG contour and the blue solid contour represents the fit ellipse for the PS contour.

model of the HG and PS. For SDSS J135711.99−070430.3, an additional Sérsic function was used to describe an interacting galaxy.

Finally, we successfully applied DECA to the sample galaxies, using the created stacked *gri*-images and their masks. In Fig. 2 we show the results of the fitting for SDSS J091558.60+093455.3. The difference of the apparent position angle of the polar structure and the host galaxy (ΔP.A.), which were retrieved from the DECA fitting, are presented in Table 1.

In addition, we provide the diameters of the host galaxy $D_{\rm HG}$ and the polar structure $D_{\rm PS}$ which were derived from the residual image 'galaxy – ring structure' and 'galaxy – host', respectively. The outermost isophotes of each residual image were plotted at the 2σ background level (which corresponds to a surface brightness of $\mu_r \approx 25.5$–26 mag arcsec^{-2}) and then fitted with ellipses with the major axes $D_{\rm PS}$ and $D_{\rm HG}$ (see Fig. 3).

Fig. 4 provides the $g - i$ colour maps for several PRG candidates. Generally, the sample galaxies are faint and small. Thus, in most cases their colour maps are irregular and noisy. We show in Fig. 4 some best examples. As one can see in the figure, the HGs look rather red while the PSs are generally bluer.

3 DISCUSSION

3.1 General characteristics of PRGs

In this section we compare characteristics of our sample galaxies with that of Smirnova & Moiseev (2013). Smirnova & Moiseev (2013) presented the combined sample of 'best candidates' from the SPRC (70 galaxies) and of eight kinematically confirmed PRGs

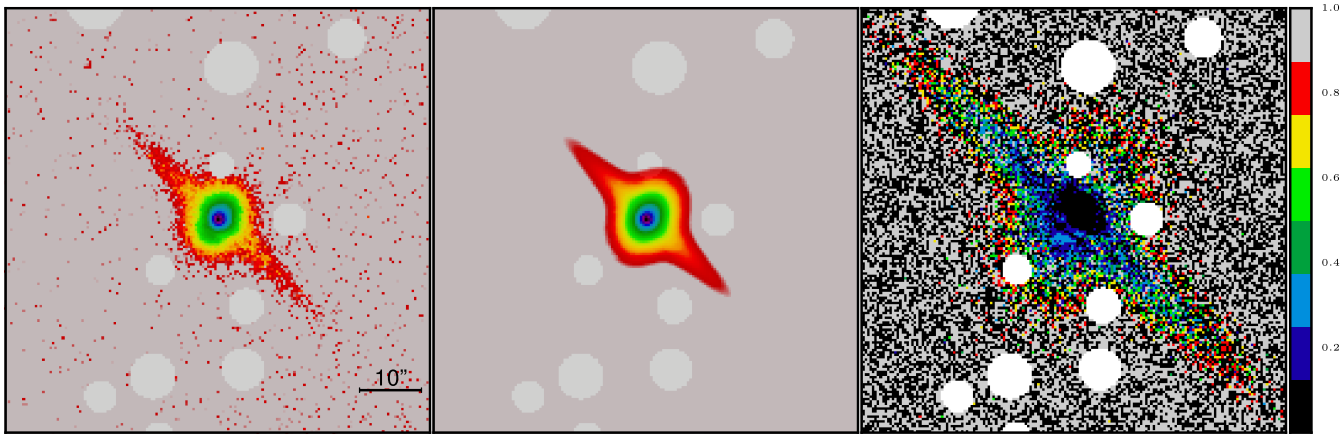

Figure 2. The results of the fitting for SDSS J091558.60+093455.3 for a stacked *gri*-image: the stacked *gri*-image (left-hand panel), the best-fitting image (middle panel), and the residual image (right-hand panel) which indicates the relative deviation between the fit and the image in absolute values, i.e. $|data - model|/model$. The right colour bar shows the scaling of the residual image. The masked objects are highlighted by the white colour. The galaxy and model images are given in a logarithmic scale. All images cover a field of view of 1 × 1 arcmin.

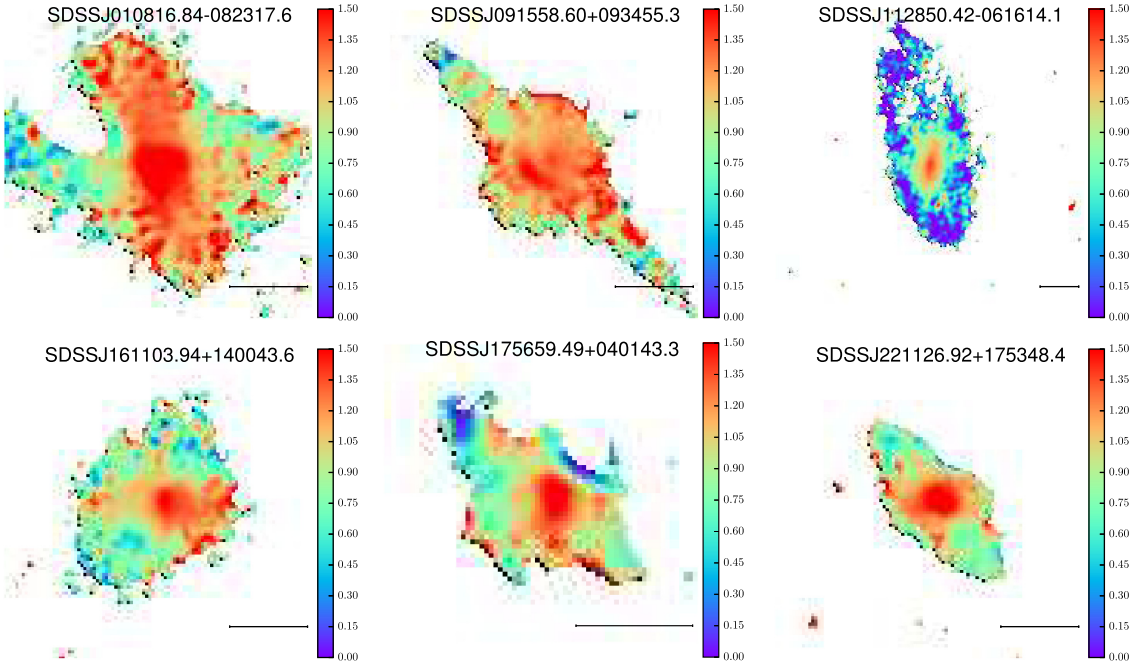

Figure 4. The $g - i$ colour maps for six candidates to PRGs. The images are limited to a 2σ-level isophote created for their corresponding *gri*-images. The scale bar in each plot corresponds to 10 arcsec.

from the SPRC and PRC catalogues with available SDSS images. The authors carried out measurements of the shape, sizes, and position angles of the host galaxy and the polar structure. At present, this is the largest published sample with the homogeneous estimates of the PRGs geometrical characteristics. Our method for measuring the PRGs sizes and position angles (see previous section) provides close results compared to those from Smirnova & Moiseev (2013).

In Fig. 5 (panels a–c), we show the comparison of the distributions by the apparent magnitude, the redshift, and the absolute magnitude of galaxies from Smirnova & Moiseev (2013) and from our Table 1. As one can see, both samples demonstrate quite close distributions. Our PRG candidates show approximately the same apparent magnitudes, redshifts, and luminosities. Thus, we can consider our sample as a notable supplement to the sample of already known PRGs selected from the SDSS.

Fig. 5d illustrates the standard observational selection effect – among distant objects we choose only the brightest. The dashed lines in the figure distinguish two subsamples: nearby PRGs with $z \leq 0.03$ (the vertical line) and bright galaxies with $M_r \leq -21$ (the horizontal line). Both subsamples are almost not intersecting.

In Table 2 we compare average characteristics of PRGs in three sets of data. Designation 'all' in the table means a joint sample (this work + Smirnova & Moiseev 2013), the 'nearby' and 'bright' ones include only galaxies with $z \leq 0.03$ or $M_r \leq -21$, respectively, from the joint sample. As one can see, typical PRGs are rather bright galaxies. Their average rest-frame integral colour $g - r$ corresponds well to early-type (S0) galaxies (e.g. Fukugita et al. 2007). Polar features are large-scale structures with typical sizes ∼20–30 kpc and their orientation is close to orthogonal with respect to the host galaxies. (The angle i in Table 2 is an apparent angular distance away from perpendicularity of the host galaxy and the ring: $i = 90^\circ - \Delta$P.A.) For the majority of PRGs, the diameter of the ring exceeds the size of the host galaxy: >70 per cent of PRGs show the ratio $D_{\rm PS}/D_{\rm HG} > 1$.

Effective radii of the sample galaxies reach several kiloparsecs (Table 1), which is typical for bright early-type galaxies. In the plane M_r–$R_{\rm eff}$ the PRG candidates are located in the area where the characteristics of previously known PRGs are resided (see fig. 4 in Reshetnikov & Combes 2015).

Our method of the surface brightness enhancement (Section 2.2) allowed us to study faint structures around the PRG candidates. According to numerical simulations, different formation mechanisms predict different external morphology of PRGs. For instance, the merger scenario leads to a faint stellar halo surrounding the PRG, while the accretion scenario does not (Bournaud & Combes 2003). Our study of the PRG images shows that almost half of the objects (14 out of 31) can be surrounded by a weak ($\mu_r \sim$ 26–26.5 mag arcsec^{-2}) envelope (see several examples in Fig. A1: SDSS 010816.84−082317.6, SDSS 041557.96−051655.8, SDSS 161103.94+140043.6, and SDSS 234407.32+253657.7). This statistics is very preliminary and is based on insufficiently deep observational data. But it shows that the merger scenario can make an appreciable contribution to the formation of PRGs. Future deep photometric observations of PRGs should clarify this issue.

3.2 The luminosity–size relation

In Fig. 6, we show the luminosity–size relation for the host galaxies and for the polar structures. As one can see, the central objects of PRGs show a tight correlation between the luminosity and diameter (Fig. 6a). The best-fitting line for our joint sample is $\log D_{\rm HG} = -0.163\,M_r - 2.21$ (the solid line in the figure). The PRGs follow this relation with an rms scatter of 0.13. The dashed line in Fig. 6a is the average relation for nearby galaxies of all morphological types (van

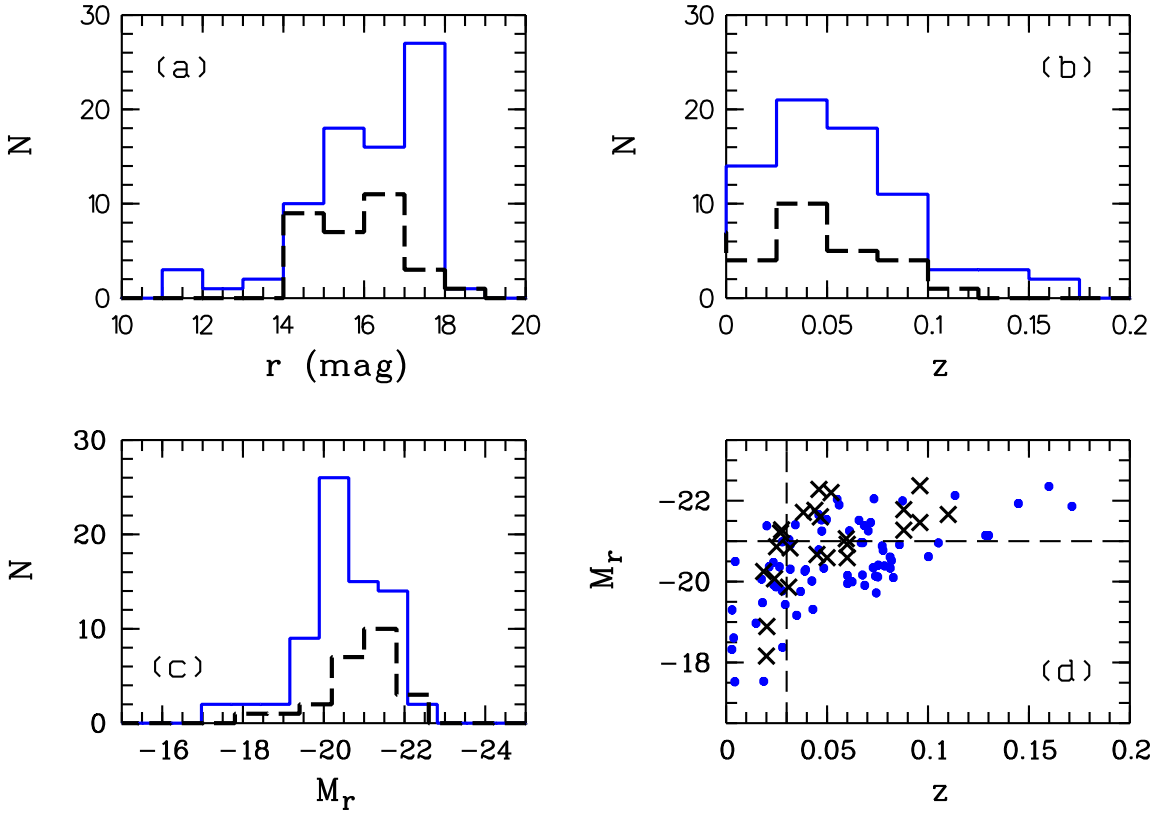

Figure 5. Histograms of the distributions of PRG candidates by (a) apparent *r*-band magnitude, (b) redshift, (c) absolute magnitude for the Smirnova & Moiseev (2013) (the blue solid line) and our (the dashed line) sample. Panel (d) shows the dependence of absolute magnitude of PRGs on their redshift (the blue points – data from Smirnova & Moiseev (2013), the crosses – data from Table 1). The dashed lines separate the two subsamples (see the text).

Table 2. Average characteristics of PRGs.

	All	Nearby $z \leq 0.03$	Bright $M_r \leq -21^m$
Number	109	26	35
z	0.055 ± 0.034	0.019 ± 0.009	0.073 ± 0.039
M_r	–20.6 ± 1.0	–19.7 ± 1.1	–21.6 ± 0.4
$(g-r)_0$	+ 0.73 ± 0.15	+ 0.72 ± 0.20	+ 0.74 ± 0.12
i (°)	16.4 ± 14.0	25.8 ± 16.9	15.4 ± 12.4
D_{HG} (kpc)	15.8 ± 7.9	11.2 ± 5.2	22.1 ± 8.3
D_{PS} (kpc)	23.3 ± 12.9	17.5 ± 11.2	27.0 ± 10.7
D_{PS}/D_{HG}	1.60 ± 0.89	1.74 ± 1.18	1.32 ± 0.64

den Bergh 2008) shifted from the *B* passband to the *r* according to Cook et al. (2014). Interestingly, HGs of PRGs follow this relation well.

The same relation but for the diameter of the polar structure is shown in Fig. 6b. The PSs follow the relation with approximately the same angle but it is shifted to higher sizes. At a given total luminosity of PRGs, polar rings are, on average, larger in comparison with their host galaxies. It is a natural result, since the direct comparison of the two subsystems gives $D_{PS}/D_{HG} > 1$ (see Table 2).

More interestingly, the PSs display a notable larger scatter around the average trend (rms dispersion is 0.20) compared to the hosts (Fig. 6a). The increasing scatter can be a direct consequence of a secondary origin of polar structures. Polar features are relatively young and they are formed during non-stationary external processes (accretion, merging). Therefore, at an early stage of formation, these structures can be asymmetric and perturbed (see e.g. Brook et al. 2008 simulations.) In the course of the subsequent evolution the secondary subsystems are likely to settle into a narrower luminosity–size relation.

3.3 The distribution of angles between the rings and the central galaxies

Previous attempts to investigate statistics of apparent angles between the rings and the host galaxies were based on relatively small samples (Whitmore 1991, Reshetnikov & Combes 2015). We prefer to investigate the apparent angle between these two subsystems, rather than to analyse the spatial angle, as done in Smirnova & Moiseev 2013, since in their case we have to know the intrinsic flattening and the shape of the two components. But now we can consider much more data. In Fig. 7 we summarize the data from Table 1 (31 galaxies, the dotted line) and from Smirnova & Moiseev (2013) (78 PRGs, the dashed line). Also, we added 28 measurements from Whitmore (1991) and constructed the final distribution for 137 PRGs (the solid histogram). Our final sample includes, thus, 137 original objects, without duplicates.

As one can see in Fig. 7, the majority of PRGs, indeed, show almost orthogonal outer structures. From the combined sample of 137 objects we conclude that 50 per cent of the PRGs demonstrate $i \leq 10°$, 75 per cent – $i \leq 23°$, and 90 per cent – $i \leq 35°$. If we consider a relatively complete subsample with $z \leq 0.03$ (26 PRGs from the joint sample Table 1 + Smirnova & Moiseev 2013 and 12 galaxies from Whitmore 1991), the distribution becomes wider: 50 per cent of the PRGs with $i \leq 17°$, 75 per cent – $i \leq 33°$, and 90 per cent – $i \leq 41°$.

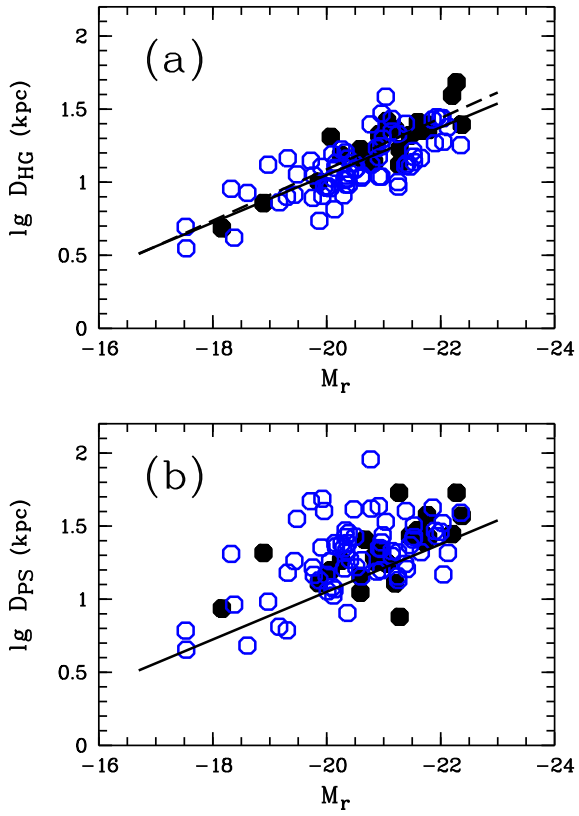

Figure 6. Absolute magnitude of the PRG versus (a) diameter of the HG or (b) diameter of the PS (the solid circles – the data from Table 1, the open circles – the characteristics of PRGs from Smirnova & Moiseev 2013). The dashed line presents the relation for nearby galaxies according to van den Bergh (2008). The solid lines in both figures show a linear approximation for the central galaxies of PRGs.

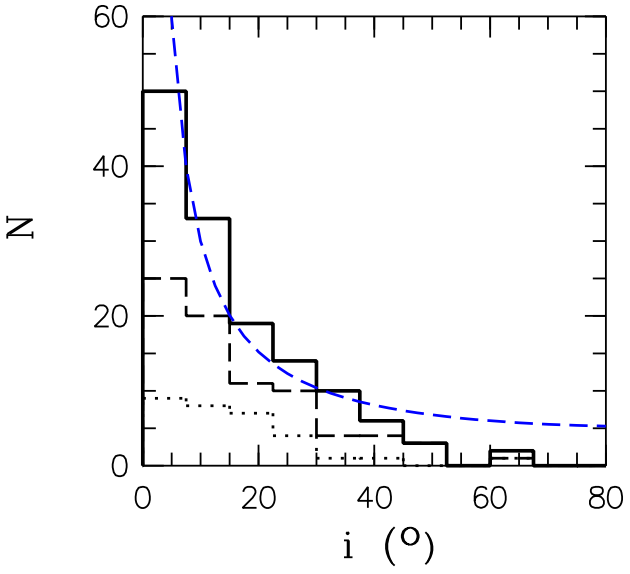

Figure 7. The distribution of PRGs as a function of the angle between the PS and the perpendicular to the disc of the central galaxy. The dotted line shows the data for our sample (Table 1), the dashed histogram – the Smirnova & Moiseev (2013) measurements, the solid line – all available data. The dashed curved line illustrates the arbitrary scaled dependence $\propto 1/\sin i$ (see the text for details).

Interpretation of the distribution by i is not a trivial task since it is not a true angle between the central galaxy plane and the plane of the PS but merely an apparent, projected angle. Moreover, the distribution in Fig. 7 is strongly affected by the observational selection.

For illustrative purposes, we placed in Fig. 7 the expected dependence of the settling time for a gaseous ring on its inclination to the preferred, stable plane (the blue dashed curve). This settling time is inversely proportional to cosine of an angle by which the ring is tilted out of a stable plane (e.g. Tohline 1990). If we assume that the plane of the HG defines the preferred plane, this dependence transforms to $1/\sin i$. It is evident from the figure that the observed distribution does approximately follow this law. For the rings with small i (nearly polar), the settling time can be long and we can observe a lot of such systems in the Universe. For more inclined structures, the rings ought to settle relatively rapidly and we have less chances to observe such objects.

4 CONCLUSIONS

In our work we presented a new sample of 31 candidates for PRGs. The galaxies were selected on the basis of their morphology from the SDSS. Our list of PRGs is a valuable addition to the SPRC catalogue (Fig. 5).

From the analysis of general characteristics of PRGs we derived the following main conclusions:

(1) The host galaxies of PRGs follow the luminosity–size relation for normal galaxies. The polar structures show similar relation but with a larger scatter (Fig. 6). This enhanced scatter may be a consequence of a secondary origin of polar rings.

(2) A nearly polar orientation dominates among the rings of PRGs: approximately half of all PRGs demonstrate extended structures within 20° from perpendicularity (Fig. 7).

On the basis of the surface brightness enhancement we tried to detect faint structures around the PRG candidates. The obtained results are uncertain (Section 3.1). Possible existence of outer stellar envelopes around PRGs is a subject of our future study.

A gradual increase of discovered PRGs makes it possible to pose new interesting questions about the nature and origin of these unique objects. One can hope that these galaxies will be put soon into the general picture of the formation and evolution of galaxies.

ACKNOWLEDGEMENTS

We thank anonymous referee for helpful constructive comments that improved the paper.

AM expresses gratitude for the grant of the Russian Foundation for Basic Researches number mol_a 18-32-00194.

This research has made use of the NASA/IPAC Extragalactic Database (NED) which is operated by the Jet Propulsion Laboratory, California Institute of Technology, under contract with the National Aeronautics and Space Administration.

Funding for the SDSS has been provided by the Alfred P. Sloan Foundation, the Participating Institutions, the National Science Foundation, the U.S. Department of Energy, the National Aeronautics and Space Administration, the Japanese Monbukagakusho, the Max Planck Society, and the Higher Education Funding Council for England. The SDSS Web Site is http://www.sdss.org/.

REFERENCES

Alam S. et al., 2015, ApJS, 219, 12
Bekki K., 1997, ApJ, 490, L37
Bekki K., 1998, ApJ, 499, 635
Bertin E., Arnouts S., 1996, A&AS, 117, 393
Bertin E., Mellier Y., Radovich M., Missonnier G., Didelon P., Morin B., 2002, in Bohlender D. A., Durand D., Handley T. H., eds, ASP Conf. Ser. Vol. 281, Astronomical Data Analysis Software and Systems XI. Astron. Soc. Pac., San Francisco, p. 228
Bournaud F., Combes F., 2003, A&A, 401, 817
Brook Ch. B., Governato F., Quinn Th., Wadsley J., Brooks A. M., Willman B., Stilp A., Jonsson P., 2008, ApJ, 689, 678
Brosch N., Kniazev A. Yu., Moiseev A., Pustilnik S. A., 2010, MNRAS, 401, 2067
Chilingarian I. V., Melchior A.-L., Zolotukhin I. Yu., 2010, MNRAS, 405, 1409
Coccato L., Iodice E., Arnaboldi M., 2014, A&A, 569, A83
Cook D. O. et al., 2014, MNRAS, 445, 890
Finkelman I., Funes J. G., Brosch N., 2012, MNRAS, 422, 2386
Fukugita M. et al., 2007, AJ, 134, 579
Gunn J. E. et al., 1998, AJ, 116, 3040
Iodice E., 2014, in Iodice E., Corsini E. M., eds, ASP Conf. Ser. Vol. 486, Narrow Polar Rings versus Wide Polar Ring/Disk GalaxiesNarrow Polar Rings versus Wide Polar Ring/Disk Galaxies. Astron. Soc. Pac., San Francisco, p. 39
Iodice E., Arnaboldi M., Sparke L. S., Freeman K. C., 2002, A&A, 391, 117
Iodice E. et al., 2015, A&A, 583, A48
Lintott C. J. et al., 2008, MNRAS, 389, 1179
Maccio A. V., Moore B., Stadel J., 2006, ApJ, 636, L25
Miskolczi A., Bomans D. J., Dettmar R.-J., 2011, A&A, 536, A66
Moiseev A., Khoperskov S., Khoperskov A., Smirnova K., Smirnova A., Saburova A., Reshetnikov V., 2015, Balt. Astron., 24, 76
Moiseev A. V., Smirnova K. I., Smirnova A. A., Reshetnikov V. P., 2011, MNRAS, 418, 244
Mosenkov A. V., 2014, Astrophys. Bull., 69, 99
Mosenkov A. V. et al., 2018, A&A, preprint (arXiv:1811.08923)
Muñoz-Mateos J. C. et al., 2015, ApJS, 219, 3
Reshetnikov V., Combes F., 2015, MNRAS, 447, 2287
Reshetnikov V., Sotnikova N., 1997, A&A, 325, 933
Reshetnikov V. P., Hagen-Thorn V. A., Yakovleva V. A., 1994, A&A, 290, 693
Reshetnikov V. P., Faúndez-Abans M., de Oliveira-Abans M., 2011, Astron. Lett., 37, 171
Schlafly E. F., Finkbeiner D. P., 2011, ApJ, 737, 103
Sérsic J. L., 1968, Atlas de Galaxias Australes. Observatorio Astronomico, Cordoba
Smirnova K. I., Moiseev A. V., 2013, Astrophys. Bull., 68, 371
Smirnova K. I., Wiebe D. S., Moiseev A. V., 2017, Open Astron., 26, 88
Spavone M., Iodice E., Arnaboldi M., 2015, MNRAS, 450, 998
Tohline J. E., 1990, New York Acad. Sci. Ann., 596, 198
van den Bergh S., 2008, A&A, 490, 97
van Driel W., Arnaboldi M., Combes F., Sparke L. S., 2000, A&AS, 141, 385
van Gorkom J. H., Schechter P. L., Kristian J., 1987, ApJ, 314, 457
Whitmore B. C., 1991, in Casertano S., Sackett P. D., Briggs F. H., eds, Warped disks and inclined rings around galaxies. Cambridge Univ. Press, Cambridge, p. 60
Whitmore B. C., McElroy D. B., Schweizer F., 1987, ApJ, 314, 439
Whitmore B. C., Lucas R. A., McElroy D. B., Steiman-Cameron T. Y., Sackett P. D., Olling R. P., 1990, AJ, 100, 1489

APPENDIX: REDUCED GALAXY IMAGES

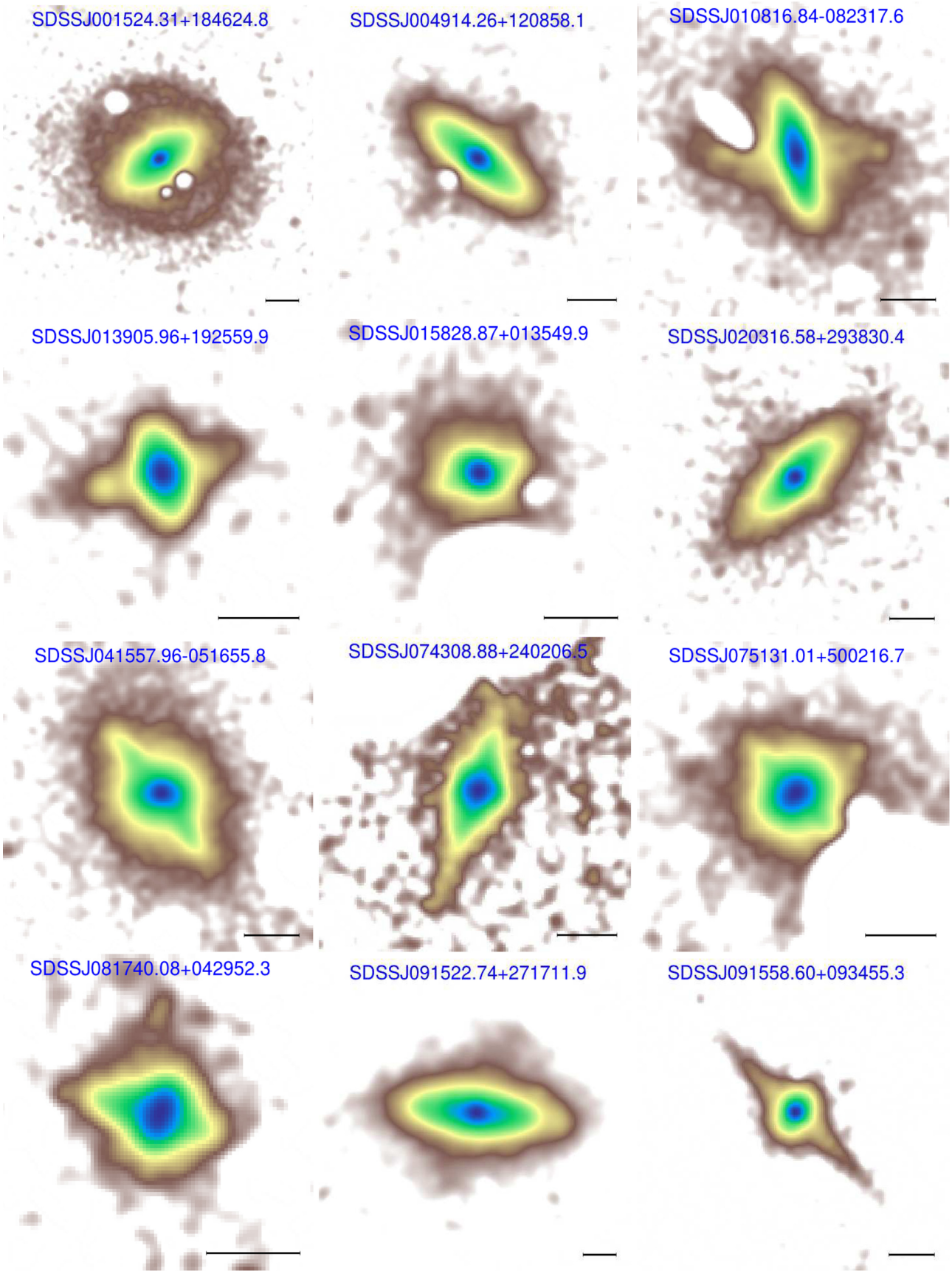

Figure A1. Reduced (stacked) *gri*-images of the candidates to PRGs. The contaminating sources have been masked. The scale bar in each plot corresponds to 10 arcsec.

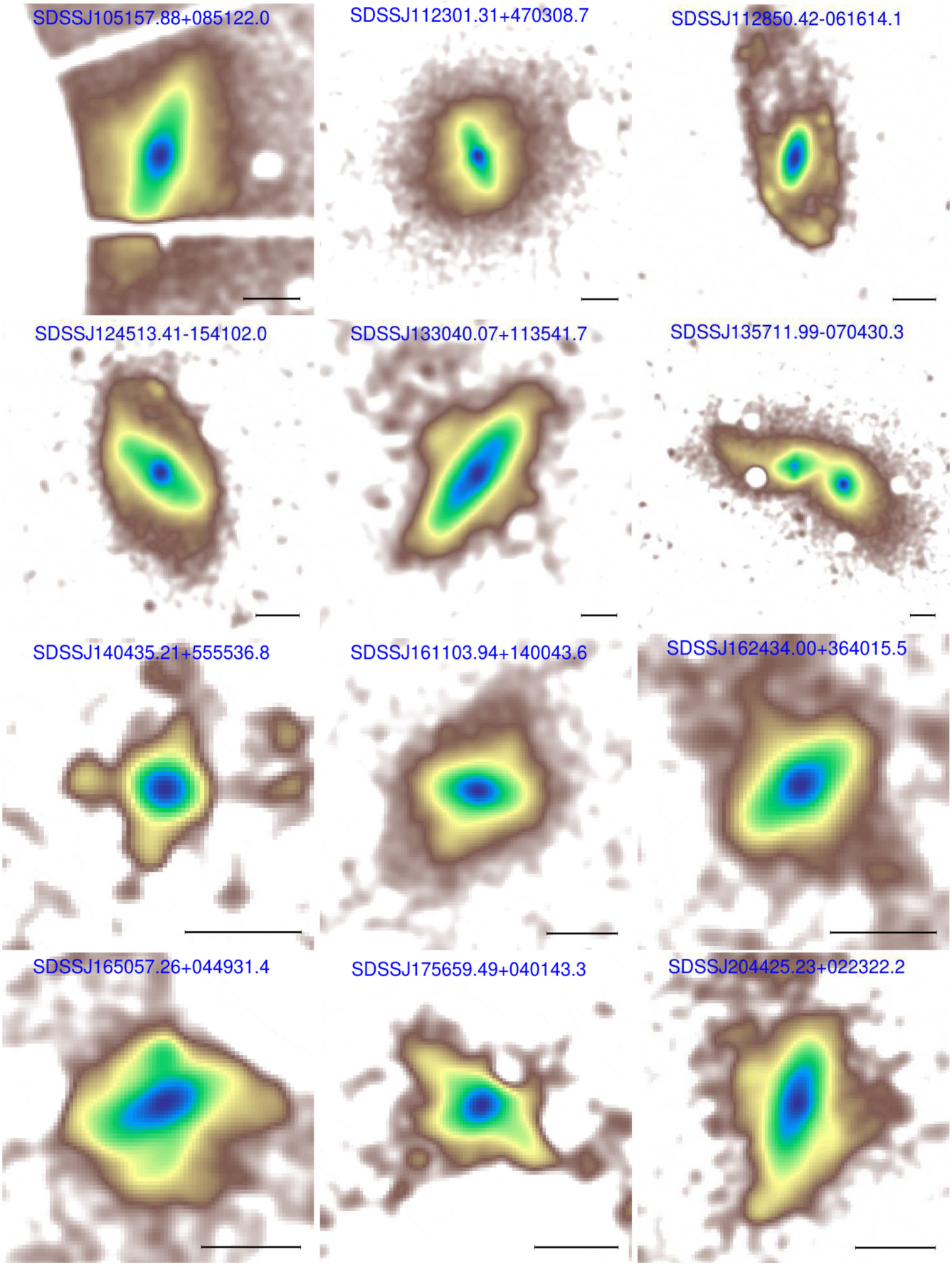

Figure A1 – *continued*

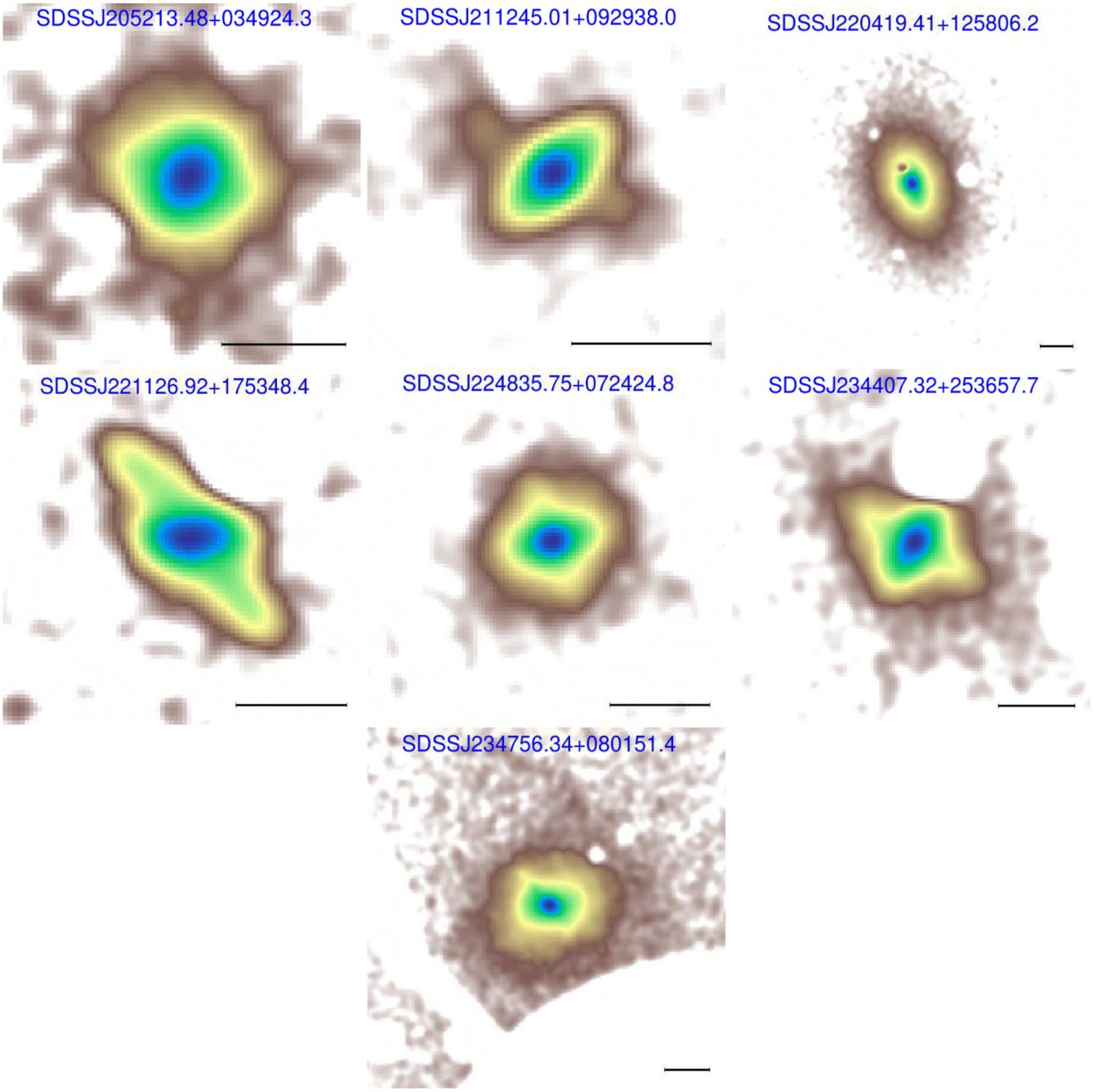

Figure A1 – *continued*

This paper has been typeset from a TEX/LATEX file prepared by the author.